

Photoluminescence of Carbon Nanodots: Dipole Emission Centers and Electron–Phonon Coupling

Siddharth Ghosh,[†] Anna M. Chizhik,[†] Narain Karedla,[†] Mariia O. Dekaliuk,[‡] Ingo Gregor,[†] Henning Schuhmann,[§] Michael Seibt,[§] Kai Bodensiek,[†] Iwan A. T. Schaap,[†] Olaf Schulz,[†] Alexander P. Demchenko,[‡] Jörg Enderlein,^{*,†} and Alexey I. Chizhik^{*,†}

[†]III. Institute of Physics, Georg August University, 37077 Göttingen, Germany

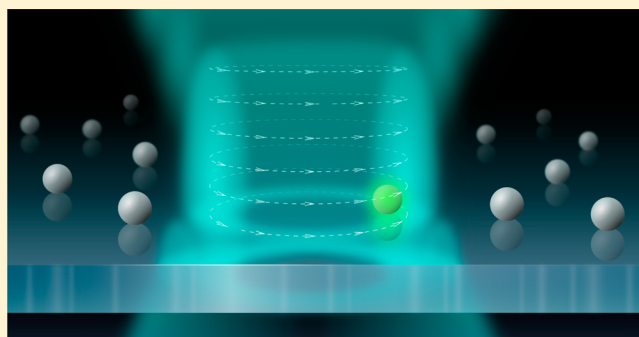
[‡]A. V. Palladin Institute of Biochemistry, National Academy of Sciences of Ukraine, Leontovicha Street 9, Kiev 01601, Ukraine

[§]IV. Institute of Physics, Georg August University, 37077 Göttingen, Germany

Supporting Information

ABSTRACT: Inorganic carbon nanomaterials, also called carbon nanodots, exhibit a strong photoluminescence with unusual properties and, thus, have been the focus of intense research. Nonetheless, the origin of their photoluminescence is still unclear and the subject of scientific debates. Here, we present a single particle comprehensive study of carbon nanodot photoluminescence, which combines emission and lifetime spectroscopy, defocused emission dipole imaging, azimuthally polarized excitation dipole scanning, nanocavity-based quantum yield measurements, high resolution transmission electron microscopy, and atomic force microscopy. We find that photoluminescent carbon nanodots behave as electric dipoles, both in absorption and emission, and that their emission originates from the recombination of photogenerated charges on defect centers involving a strong coupling between the electronic transition and collective vibrations of the lattice structure.

KEYWORDS: carbon nanodots, electron–phonon coupling, fluorescence, nanoparticles, nanotechnology, transition dipole moment



During the past decades, a large number of new nanostructured carbon-based materials with unique and unexpected physicochemical properties have been discovered. Among them are nanodiamonds, fullerenes, graphene, carbon nanotubes, as well as an endless variety of their combinations.¹ Recently, a new type of carbon-based material has attracted considerable scientific attention. Carbon nanoparticles, which are frequently called carbon nanodots (CNDs) by analogy with semiconductor nanocrystals, have been first obtained during purification of single-walled carbon nanotubes through preparative electrophoresis by Scrivens and co-workers in 2004.² CNDs immediately became the topic of numerous scientific studies because of their unique combination of bright photoluminescence (PL), high aqueous solubility, easy functionalization, low toxicity, high photostability, and chemical inertness.^{3–6} This, along with a simple and inexpensive one-step synthesis^{7–9} allowed CNDs to find applications in biological imaging,¹⁰ drug delivery,¹¹ sensing,¹² photovoltaic devices,¹³ lasing,¹⁴ or catalysis.¹⁵ Recently, it has been shown that CNDs are also a promising material for fabrication of flexible electroluminescent devices, solid-state lighting, color displays, and luminescent solar concentrators.¹⁶

Despite the rapidly growing number of investigations that try to understand the fundamental mechanism of their PL, many

details of basic photophysical and spectroscopic properties of CNDs are still unclear. For instance, ensemble emission spectroscopic studies on CNDs indicate that the PL spectrum shifts depending on excitation wavelength,⁴ which suggests that fluorescent CNDs include multichromophoric units. However, it is not known whether the multiple emissive centers are present within a single particle or originate from separate particles. Such information cannot be gained from ensemble measurements that capture only the average values of CNDs' size, shape, or the presence of chemical defects. Recently, it has been shown that the emissive properties of CNDs are sensitive to surface passivation and solvent pH.¹⁷ A small number of existing single particle PL studies revealed controversial observations of the PL intermittency character, which varied from moderate blinking¹⁸ to its full absence.¹⁹ Thus, the complex diversity of the reported observations makes it hard to reveal the PL origin of the CNDs, which is one of the key issues of ongoing discussions.

Here, we present results that provide fundamentally new insight into the PL mechanism of single CNDs and its relation

Received: June 25, 2014

Revised: September 19, 2014

Published: September 23, 2014

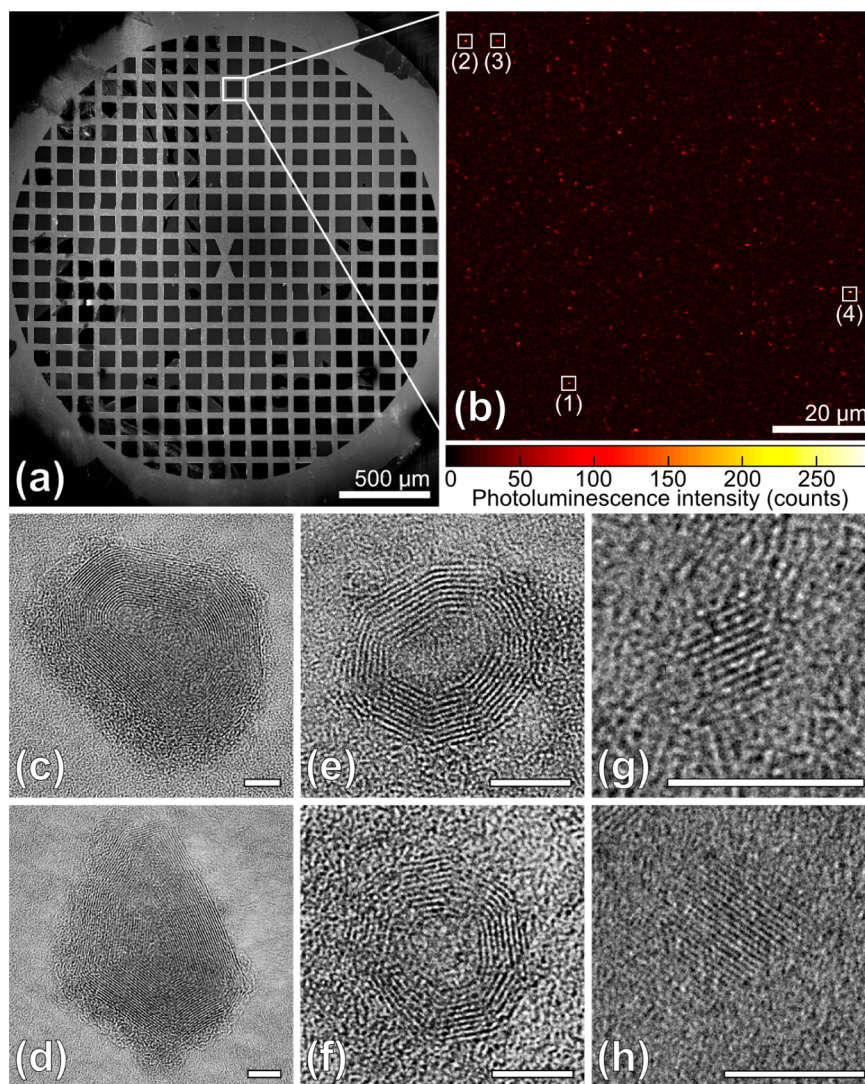


Figure 1. (a) Scanning electron microscopy image of a the carbon/copper grid, used for PL-correlated TEM imaging. (b) PL confocal scanning image recorded in one of the grid sections. (c)–(h) HRTEM images of individual CNDs possessing various crystal structures and shapes. Localization of the CNDs on the PL image: (c) and (d) two bright spots in area 1; (e) and (f) bright spots in areas 2 and 3, respectively; (g) and (h) two bright spots in area 4. The white bars at the right bottom corners of (c)–(h) are 5 nm scale bars.

to their structural properties, by combining various single-particle optical spectroscopic methods with high resolution transmission electron microscopy (HRTEM) on the same CNDs, and with atomic force microscopy (AFM). For a correlative measurement of the luminescence properties, crystal structure, and shape of single CNDs, we combined PL imaging and spectroscopy with HRTEM of the same sample. The particles were dispersed on the surface of a standard carbon/copper TEM grid, shown in Figure 1a. For the PL measurements, the grid was placed on the surface of a clean glass cover slide to avoid contact of the grid with the immersion oil of a high numerical aperture objective lens. An exemplary PL image obtained by confocal scanning of one of the grid sections is shown in Figure 1b. Then, HRTEM measurements were performed in areas where the PL image exhibited bright spots, corresponding to individual luminescent CNDs.

Figure 1c–h shows HRTEM images of the observed nanostructures. They can be subdivided into the two types of particles. The first type of particles, shown in Figure 1c–f, possesses a lattice spacing of around 0.35–0.36 nm, which agrees well with the $\langle 002 \rangle$ plane of graphitic carbon⁶ (we will

call it crystal structure I). The observed nanostructures have different diameters varying from near 20 to 7 nm, different aspect ratios from near 1.5 (Figure 1c,d) to 1 (Figure 1e,f), and characteristic onion-like shape structure.²⁰ Their localization in the PL image (Figure 1b) corresponds to the bright spots in areas 1, 2, and 3, respectively. The second type of CNDs, observed in the HRTEM images is characterized by fully crystalline particles, with 2–5 nm in diameter (Figure 1g,h). The lattice spacing of nearly 0.24 nm corresponds to the $\langle 100 \rangle$ crystal plane of graphite⁶ (crystal structure II). All the observed CNDs are composed of multiple layers of graphene, as determined by recording electron diffraction patterns (see Supporting Information). Similar carbonic nanostructures have been observed in other studies using alternative top-down or bottom-up synthetic methods (see 5 and 6 and citations therein). Some of the CNDs that possessed an onion-like shape structure exhibited an amorphous carbon shell. Using energy-dispersive X-ray spectroscopy, we found that the shells are mainly composed of oxygen and carbon atoms and can be attributed to C=O and –OH groups, which have been

frequently observed in previous studies²¹ (see Supporting Information for further details).

With the AFM setup, we have recorded images of CNDs dispersed on the surface of a glass cover slide by spin coating a droplet of an aqueous solution of CNDs. In order to do a comparative study of the CNDs, we employed the same method of sample preparation for AFM as for HRTEM and PL imaging, but using a ten times higher concentration of CNDs in solution. A representative image of a $10 \times 10 \mu\text{m}^2$ area containing 244 CNDs is shown in Figure S4a of the Supporting Information. The image exhibits a homogeneous distribution of CNDs with an average height of the order of several nanometers. The observed lateral dimension of the particles is limited by the size of the AFM tip. Figure S4b of the Supporting Information shows a histogram of the observed CNDs height vs the number of particles. Whereas the size of the majority of CNDs does not exceed 6 nm, several particles with a size of up to 15 nm were detected. The distribution of CND height values obtained from AFM measurements is shifted toward smaller values as compared with the axial dimensions measured in HRTEM (2–20 nm). This shows that despite the quasispherical shape of the particles, observed in most of the HRTEM images, some of the CNDs have an oblate shape. The fact that we detect comparable number of the particles per sample area in AFM (taking into account the initial concentration of CNDs in solution), HRTEM, and PL studies suggests that most of the CNDs are optically active.

One of the key parameters of any single quantum emitter is its transition dipole moment (TDM). It has been shown that depending on the origin of PL in semiconductor nanocrystals^{22–25} and dielectric nanoparticles,²⁶ the dimensionality of emission and excitation TDMs changes. For instance, both the excitation and emission TDMs of spherical silicon nanocrystals coated with a SiO_2 amorphous shell are distributed in one- or three- dimensions, depending on whether their PL originates from surface defects or from a quantum-confined electron–hole pair, respectively.²⁵

A straightforward way for measuring the orientation and dimensionality of the excitation TDM is scanning an emitter through the focal region of an azimuthally polarized laser beam (APLB).^{24,27} Figure 2a shows excitation patterns of individual CNDs dispersed on the surface of a glass cover slide. All of the recorded patterns consist of two nearby bright spots of elliptical shape, which corresponds to a fixed linear excitation TDM. The projection of the TDM on the substrate surface is oriented along the dark gap in the middle of the double-lobe pattern, as shown in the inset of Figure 2a. Out-of-plane orientations of the dipole moment lead to a weaker intensity of the double-lobe pattern, whereas dipole moments oriented exactly perpendicular to the surface cannot be observed at all.

Figure 2b–g shows a series of successive single CND excitation patterns. Acquisition time for one image was 6 s. A small asymmetry of the double-lobe pattern is caused by a slight distortion of the excitation laser beam. Fixed orientation of the pattern indicates that the TDM did not undergo reorientation during the acquisition time. Because excitation patterns are obtained by point scanning, a dark line in Figure 2d indicates PL intermittency. A single step transition from an on-state to background in PL intensity as shown in Figure 2f corresponds to single step bleaching of CND PL. The single step transition of the PL between the on- and off-state indicates that the observed emission originates from a single quantum emitter.

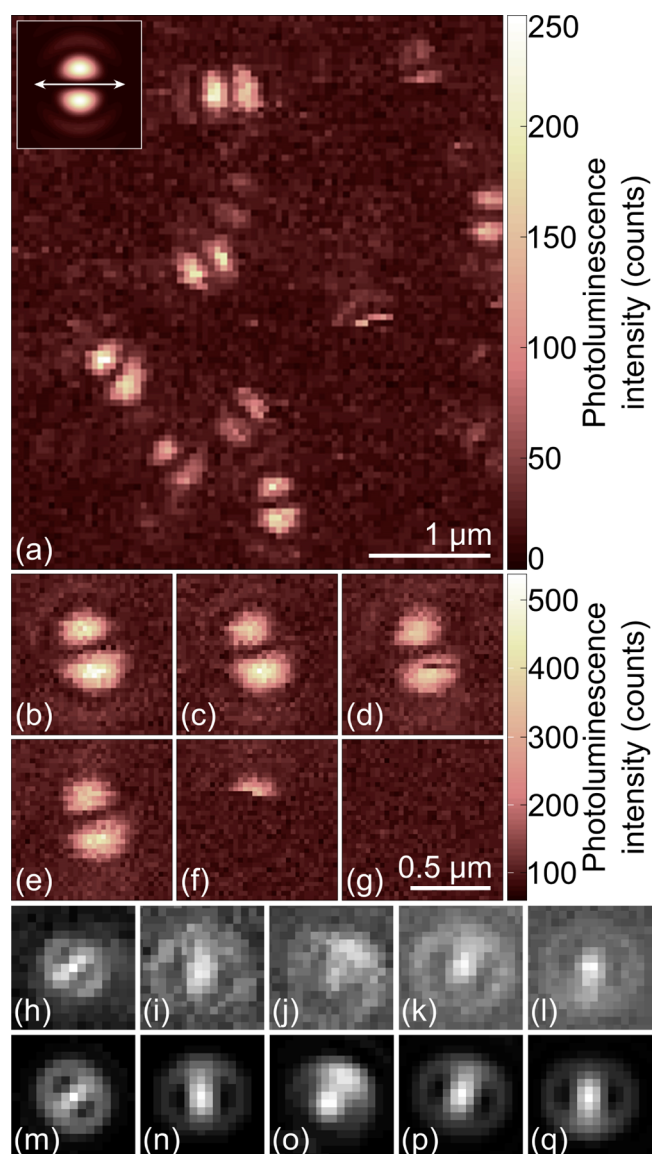


Figure 2. (a) Single CNDs excited with an azimuthally polarized laser beam. Inset shows a theoretically calculated excitation pattern for identical experimental conditions assuming a linear horizontal dipole. The orientation of the dipole is indicated by the double arrow. (b)–(g) Consecutive images of the same sample area recorded by using an azimuthally polarized laser beam (scanning direction up–down). Each double-lobe pattern corresponds to the same CND. The images show PL intermittency (d) and single-step photobleaching (f) of the particle. Scanning direction is top–down. (h)–(q) Defocused images of single CNDs: experimental data (h)–(l) and fitted patterns (m)–(q), respectively. All the patterns correspond to the emission of a single fixed dipole.

To better illustrate the PL intermittency and bleaching, which was observed on excitation patterns, we recorded PL time traces from individual CNDs (Supporting Information Figure S5). All the measured particles exhibit a single-step transition between the on- and off-states. The rare PL intermittency of the CNDs varies from short off-states close to several milliseconds to longer ones on the order of hundreds of milliseconds.

Whereas imaging with an APLB provides information about the excitation TDM, the orientation and dimensionality of the emission TDM can be determined using defocused imag-

ing.^{28,29} By moving the objective lens toward the sample and imaging the PL of single CNDs with a CCD camera, one observes a defocused image of a single CND's PL, which provides information about the angular distribution of the emission of the imaged particle. Figure 2h–l shows five exemplary PL patterns of individual CNDs recorded with defocused imaging. The defocusing values (displacement of objective toward sample) were 280 nm for Figure 2h and 300 nm for (i)–(l). Experimental images can be very well fitted with a model that assumes that the emission originates from a single fixed dipole, as shown in Figure 2m–q.²⁹ Measuring the excitation patterns and defocused images of the same individual CNDs showed that both excitation and emission transition dipoles of the particles are oriented parallel to each other within the error of the measurements. The exemplary single CND images are shown in Figure S6 of the Supporting Information.

We measured PL lifetime values of 474 individual CNDs dispersed on the surface of a glass cover slide. The histogram of the lifetime distribution is shown in Supporting Information, Figure S7. The relatively broad distribution covers a range from 0.8 to 6 ns with a maximum close to 3 ns. The dependence between PL lifetime and intensity of single CNDs is displayed in Figure S7 of the Supporting Information, showing no obvious correlation between lifetime and intensity. The PL decay curves measured from single CNDs exhibit a monoexponential character. Supporting Information Figure S8 shows three examples of measured decay curves. The monoexponential character of the single CNDs decay curves suggest that the multiexponential PL decays reported in refs 4 and 30 originate from a very broad PL lifetime distribution across an ensemble of CNDs.

Using a home-built confocal microscope, we measured PL spectra of single CNDs dispersed on the surface of a glass cover slide. Figure 3a shows spectra of different CNDs (spectra 2–5) as well as an ensemble spectrum, recorded from particles suspended in aqueous solution (spectrum 1). The full series of single CND PL spectra is given in Figure S9 of the Supporting Information. The inset shows a photograph of a vial with CNDs in water illuminated by ambient light (left) and upon excitation with a 488 nm excitation laser (right). The right picture was taken through a 500 nm long pass filter to block the scattered laser radiation. The bulk emission covers a broad spectral range centered at 550 nm (near 2.27 eV).

Individual CND spectra are much narrower than the bulk emission spectrum, and show random spectral shifts from 500 to 650 nm (near 2.5–1.9 eV) in agreement with the width of the ensemble PL spectrum. All single particle spectra are broadened toward the low-energy side, exhibiting there a second less-intense band. To calculate the energy splitting of the two bands, we fitted the single CNDs spectra by two Gaussian functions. The fit results are plotted in Figure 3a (red curves). Solid circles in Figure 3b show the separation between the two spectral lines vs the maximum of the high-energy line. The splitting varies from 70 to 150 meV and exhibits no clear dependence on the PL energy maximum.

From the knowledge of the crystal structures of single CNDs, obtained by a Fourier transform of the HRTEM data, we calculated all possible optical phonon modes using a density–function tight-binding method³¹ (see Supporting Information for further details and the full list of calculated values). Within the experimentally observed 70–150 meV energy range, three values for optical phonon modes were found: 98 (crystal structure I), 112, and 113 meV (crystal structure II). The

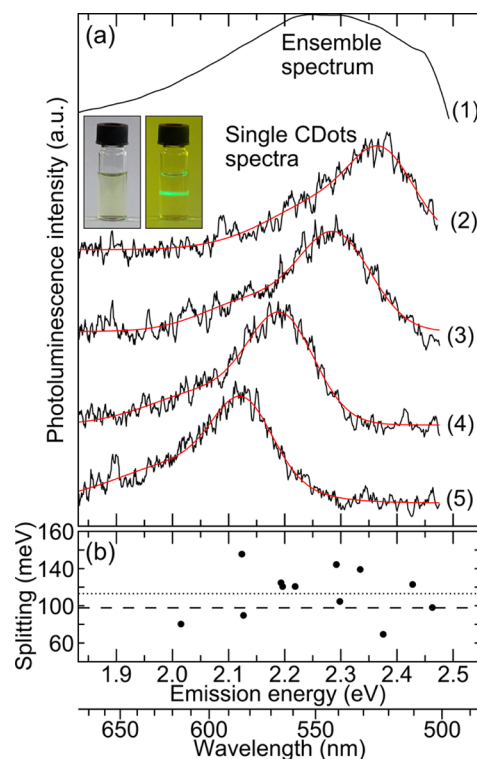


Figure 3. (a) Bulk PL spectrum of CNDs in water (spectrum 1) and exemplary PL spectra of single CNDs dispersed on the surface of a glass cover slide (spectra 2–5). Before plotting, the experimental data has been subjected to averaging over five data points. The full series of single CND PL spectra is given in the Supporting Information. Inset shows two photographs of a cuvette containing CNDs in an aqueous solution under ambient light excitation (left) and upon excitation with a 488 nm laser (right). The left photograph is taken through a 500 nm long-pass filter to block scattered laser light. (b) Splitting between zero-phonon and phonon-assisted bands for all PL spectra measured in this study as a function of zero-phonon line energy (solid circles). Dashed and dotted lines represent the result of the phonon energy calculations for the crystal structures I and II, respectively.

obtained values are shown in Figure 3b by dashed and dotted lines for the crystal structures I and II, respectively. It should be emphasized that the other theoretically obtained phonon energy values sufficiently differ and show no overlap with the experimental data. The moderate dispersion of the measured values can be attributed to the high curvature of the crystal structure, especially in the case of onion-shaped particles. Hence, we assign the lower energy satellite peak to the excitation of optical phonons, coupled to the radiative recombination of the charge carriers. Interactions between electrons and lattice vibrations result in a bound state, which leads to a decrease of energy as compared to a noninteracting system. This manifests itself in the lowering of the energy of emitted photons.³² As the CNDs were not embedded into a polymer matrix during PL measurements, the emission energy as well as the phonon energy are solely related to the structure of the particles and are not affected by any local chemical environment. A strong coupling between electronic transitions and phonons due to a relaxation mechanism involving charges has been also observed in other types of nanostructures, for example, SiO₂ nanoparticles²⁶ or Si³³ or CdSe³⁴ nanocrystals.

Recent studies have shown that the shape of the bulk PL spectrum from CNDs is strongly dependent on the excitation wavelength.⁴ To find out whether tuning of the excitation

wavelength changes the shape of a single particle PL spectrum, we measured single CNDs emission spectra using different excitation wavelengths. Figure 4 shows the normalized PL

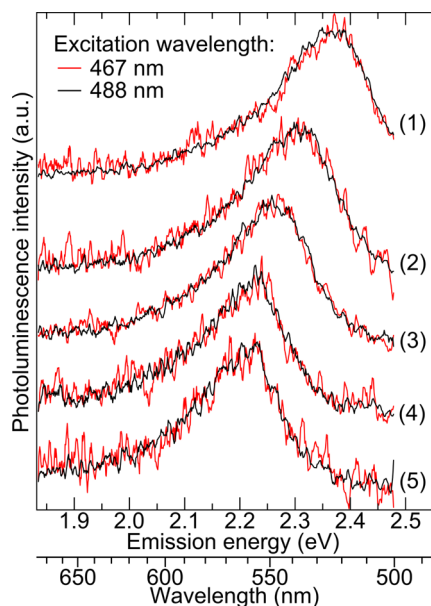


Figure 4. Normalized PL spectra of single CNDs dispersed on the surface of a glass cover slide excited with 467 nm (red curve) and 488 nm (black curve) laser beam. Before plotting, the experimental data has been subjected to averaging over five data points.

spectra recorded from five individual CNDs using 467 nm (red curve) and 488 nm (black curve) excitation laser beams. For all the measured CNDs, the shape of the emission spectra did not exhibit any noticeable change. Supporting Information Table S1 shows the values of the main emission band maxima, which were obtained as a result of fitting of the spectra with two Gaussian functions. The difference between the maxima of the spectra recorded from the same CND at different excitation wavelengths does not exceed 1%, which can be attributed to the error of fitting. This finding suggests that the wavelength-dependent modification of the ensemble PL spectrum of CNDs is caused by excitation of different subsets of CNDs due to sample heterogeneity.

The wavelength-dependent modulation of the CNDs' ensemble PL, along with the large difference between the absorption and excitation spectra, makes it difficult to use standard methods for measuring the quantum yield (QY) of CNDs. However, our recently developed nanocavity-based method of QY determination measures only the cavity-modulated radiative decay rate of an emitter,³⁵ which makes it also applicable for such complex systems as CNDs.^{36,37} Placing CNDs between the metal mirrors of a nanocavity changes their emission behavior due to a cavity-modified electromagnetic field mode density.^{38,39} Because the cavity changes only the radiative rate of the embedded emitters, measuring the modulation of the PL lifetime as a function of the cavity length allows for determining an absolute value of an emitters' QY.³⁵ Moreover, as the rotational diffusion of the emission dipoles modifies the coupling of the emitters to the cavity modes,⁴⁰ measuring the cavity-induced lifetime modification allows us also to estimate the rotational diffusion time of the CNDs.

Figure S10 of the Supporting Information shows the result of PL lifetime measurements of CNDs in a droplet of water placed into a metallic nanocavity as a function of cavity length. The solid curve shows a fit of a theoretical model to the experimental data, where the free fit parameters are the quantum yield value Φ , the rotational diffusion time τ_{rot} and the free space PL lifetime τ_0 (i.e., lifetime in aqueous solution without a cavity). The calculated free space lifetime value of 2.8 ns is in very good agreement with the average free space lifetime measured for CNDs on a glass cover slide (see Supporting Information, figure S7). The obtained quantum yield value of 19% places CNDs into the category of highly photoluminescent emitters.

The determined rotational diffusion time value allows us to estimate the size of the CNDs via the Stokes–Einstein–Debye relation.⁴¹ The measured rotational diffusion time of 16 ns corresponds to spherical particles of nearly 5 nm diameter, which is in good agreement with the average CND size obtained from the HRTEM and AFM studies.

The broad distribution of single CND brightness and PL lifetime values suggests a strong variation of the QY across different particles. We estimated the distribution of single particle QY values based on the ensemble QY measurement (Supporting Information Figure S10) and the distribution of single particle brightness and lifetime values (Supporting Information Figure S7). We found that the QY of the majority of measured CNDs lies within the range of 0–0.3; however, it can be as high as near 0.6 for the brightest particles observed, as detailed in section “Single CND quantum yield distribution” of the Supporting Information.

The observed properties of CND PL, that is, fixed linear emission and excitation TDMs, broad distribution of PL lifetimes, and random shifts of the emission spectra, resemble the PL properties of SiO₂ nanoparticles, where the emission originates from defects in the SiO₂ structure.^{26,42} The fact that the PL of CNDs with different crystal structures does not show pronounced differences is a strong indication that the emission originates from a charge recombination on defect centers on the surface of a CND, rather than originating from its core. This conclusion is supported by recent fluorescent quenching experiments on CNDs using iodide anions, which show a high accessibility of fluorescent centers by the quencher.³⁰ The homogeneous dispersion of PL spectral emission maxima and lifetime values suggests that all emission originates from the same type of defects, whereas the dispersion is induced by random fluctuations in the local structural environment.

The spectral dispersion of a single CNDs' PL and the linearity of their emission and excitation TDMs show that multiple emission centers, observed in previous studies (see 4 and citations therein), result from different particles, whereas each CND contains only one single optically active emission center. It should be emphasized that the relatively high structural heterogeneity of the studied CNDs does not lead to a similarly heterogeneous behavior in their PL.

In summary, we have presented a comprehensive PL, HRTEM, and AFM study of single CNDs, which allowed us to relate their fundamental optical and structural properties. We showed that the PL of CNDs originates from a charge recombination on surface emission centers, involving a strong coupling between the electronic transition and collective vibrational modes of the lattice structure. Whereas the PL properties of individual CNDs resemble those of typical dye molecules, the temporal and spectral dispersion of their PL

reflects the complex nature of the local chemical environment around each PL center. Finally, we showed that CNDs, which can be synthesized without the need for sophisticated and expensive equipment, possess a high PL QY and photostability, which makes them ideal candidates for luminescent centers in bioimaging.

■ ASSOCIATED CONTENT

🔍 Supporting Information

More detailed information regarding the crystal structure of CNDs, chemical analysis of CNDs, phonon frequency calculation, full list of the calculated optical phonon energies, single CND quantum yield distribution, experimental methods, and the supplementary figures and tables. This material is available free of charge via the Internet at <http://pubs.acs.org>.

■ AUTHOR INFORMATION

Corresponding Authors

*E-mail: jenderl@gwdg.de

*E-mail: alexey.chizhik@phys.uni-goettingen.de

Notes

The authors declare no competing financial interest.

■ ACKNOWLEDGMENTS

This research was supported in part by Ukraine-Germany collaboration program BMBF (project 01DK13036). Funding by the German Science Foundation (DFG, SFB 937 (project A5), SFB 1073 (project B02)) is gratefully acknowledged. A.M.C. thanks the Dorothea Schlözer Fellowship Programme for financial support. A.I.C. acknowledges financial support from the Alexander von Humboldt Foundation. S.G. and N.K. thanks the Niedersächsisches Ministerium für Wissenschaft und Kultur for a MWK stipend.

■ REFERENCES

- (1) Jariwala, D.; Sangwan, V. K.; Lauhon, L. J.; Marks, T. J.; Hersam, M. C. *Chem. Soc. Rev.* **2013**, *42*, 2824.
- (2) Xu, X.; Ray, R.; Gu, Y.; Ploehn, H. J.; Gearheart, L.; Raker, K.; Scrivens, W. A. *J. Am. Chem. Soc.* **2004**, *126*, 12736.
- (3) Bottini, M.; Mustelin, T. *Nat. Nano* **2007**, *2*, 599.
- (4) Demchenko, A. P.; Dekaliuk, M. O. *Methods Appl. Fluoresc.* **2013**, *1*, 042001.
- (5) Li, H.; Kang, Z.; Liu, Y.; Lee, S.-T. *J. Mater. Chem.* **2012**, *22*, 24230.
- (6) Baker, S. N.; Baker, G. A. *Angew. Chem., Int. Ed.* **2010**, *49*, 6726.
- (7) Jiang, J.; He, Y.; Li, S.; Cui, H. *Chem. Commun.* **2012**, *48*, 9634.
- (8) Liu, C.; Zhang, P.; Tian, F.; Li, W.; Li, F.; Liu, W. *J. Mater. Chem.* **2011**, *21*, 13163.
- (9) Hsu, P.-C.; Chang, H.-T. *Chem. Commun.* **2012**, *48*, 3984.
- (10) Qu, S.; Wang, X.; Lu, Q.; Liu, X.; Wang, L. *Angew. Chem., Int. Ed.* **2012**, *51*, 12215.
- (11) Tang, J.; Kong, B.; Wu, H.; Xu, M.; Wang, Y.; Wang, Y.; Zhao, D.; Zheng, G. *Adv. Mater.* **2013**, *25*, 6569.
- (12) Yu, C.; Li, X.; Zeng, F.; Zheng, F.; Wu, S. *Chem. Commun.* **2013**, *49*, 403.
- (13) Wang, X.; Cao, L.; Lu, F.; Mezzani, M. J.; Li, H.; Qi, G.; Zhou, B.; Harruff, B. A.; Kermarrec, F.; Sun, Y.-P. *Chem. Commun.* **2009**, 3774.
- (14) Zhang, W. F.; Zhu, H.; Yu, S. F.; Yang, H. Y. *Adv. Mater.* **2012**, *24*, 2263.
- (15) Li, H.; He, X.; Kang, Z.; Huang, H.; Liu, Y.; Liu, J.; Lian, S.; Tsang, C. H. A.; Yang, X.; Lee, S.-T. *Angew. Chem., Int. Ed.* **2010**, *49*, 4430.
- (16) Wang, Y.; Kalytchuk, S.; Zhang, Y.; Shi, H.; Kershaw, S. V.; Rogach, A. L. *J. Phys. Chem. Lett.* **2014**, *5*, 1412.

(17) Krysmann, M. J.; Kelarakis, A.; Dallas, P.; Giannelis, E. P. *J. Am. Chem. Soc.* **2012**, *134*, 747.

(18) Das, S. K.; Liu, Y.; Yeom, S.; Kim, D. Y.; Richards, C. I. *Nano Lett.* **2014**, *14*, 620.

(19) Sun, Y.-P.; Zhou, B.; Lin, Y.; Wang, W.; Fernando, K. A. S.; Pathak, P.; Mezzani, M. J.; Harruff, B. A.; Wang, X.; Wang, H.; Luo, P. G.; Yang, H.; Kose, M. E.; Chen, B.; Veca, L. M.; Xie, S.-Y. *J. Am. Chem. Soc.* **2006**, *128*, 7756.

(20) Pech, D.; Brunet, M.; Durou, H.; Huang, P.; Mochalin, V.; Gogotsi, Y.; Taberna, P.-L.; Simon, P. *Nat. Nano* **2010**, *5*, 651.

(21) Wang, L.; Zhu, S.-J.; Wang, H.-Y.; Qu, S.-N.; Zhang, Y.-L.; Zhang, J.-H.; Chen, Q.-D.; Xu, H.-L.; Han, W.; Yang, B.; Sun, H.-B. *ACS Nano* **2014**, *8*, 2541.

(22) Empedocles, S. A.; Neuhauser, R.; Bawendi, M. G. *Nature* **1999**, *399*, 126.

(23) Brus, L. E.; Szajowski, P. F.; Wilson, W. L.; Harris, T. D.; Schuppler, S.; Citrin, P. H. *J. Am. Chem. Soc.* **1995**, *117*, 2915.

(24) Chizhik, A. I.; Chizhik, A. M.; Khoptyar, D.; Bär, S.; Meixner, A. *J. Nano Lett.* **2011**, *11*, 1131.

(25) Schmidt, T.; Chizhik, A. I.; Chizhik, A. M.; Potrick, K.; Meixner, A. J.; Huisken, F. *Phys. Rev. B* **2012**, *86*, 125302.

(26) Chizhik, A. M.; Chizhik, A. I.; Gutbrod, R.; Meixner, A. J.; Schmidt, T.; Sommerfeld, J.; Huisken, F. *Nano Lett.* **2009**, *9*, 3239.

(27) Chizhik, A. I.; Chizhik, A. M.; Huss, A.; Jäger, R.; Meixner, A. J. *J. Phys. Chem. Lett.* **2011**, *2*, 2152.

(28) Jasny, J.; Sepiol, J. *Chem. Phys. Lett.* **1997**, *273*, 439.

(29) Patra, D.; Gregor, I.; Enderlein, J. *J. Phys. Chem. A* **2004**, *108*, 6836.

(30) Dekaliuk, M. O.; Viagin, O.; Malyukin, Y. V.; Demchenko, A. P. *Phys. Chem. Chem. Phys.* **2014**, *16*, 16075.

(31) Elstner, M.; Porezag, D.; Jungnickel, G.; Elsner, J.; Haugk, M.; Frauenheim, T.; Suhai, S.; Seifert, G. *Phys. Rev. B* **1998**, *58*, 7260.

(32) Martin, J.; Cichos, F.; Huisken, F.; von Borczyskowski, C. *Nano Lett.* **2008**, *8*, 656.

(33) Kovalev, D.; Heckler, H.; Ben-Chorin, M.; Polisski, G.; Schwartzkopff, M.; Koch, F. *Phys. Rev. Lett.* **1998**, *81*, 2803.

(34) Empedocles, S. A.; Neuhauser, R.; Shimizu, K.; Bawendi, M. G. *Adv. Mater.* **1999**, *11*, 1243.

(35) Chizhik, A. I.; Gregor, I.; Ernst, B.; Enderlein, J. *ChemPhysChem* **2013**, *14*, 505.

(36) Chizhik, A. I.; Gregor, I.; Enderlein, J. *Nano Lett.* **2013**, *13*, 1348.

(37) Karedla, N.; Enderlein, J.; Gregor, I.; Chizhik, A. I. *J. Phys. Chem. Lett.* **2014**, *5*, 1198.

(38) Goy, P.; Raimond, J. M.; Gross, M.; Haroche, S. *Phys. Rev. Lett.* **1983**, *50*, 1903.

(39) Chizhik, A. I.; Chizhik, A. M.; Khoptyar, D.; Bär, S.; Meixner, A. J.; Enderlein, J. *Nano Lett.* **2011**, *11*, 1700.

(40) Chizhik, A. I.; Gregor, I.; Schleifenbaum, F.; Müller, C. B.; Röling, C.; Meixner, A. J.; Enderlein, J. *Phys. Rev. Lett.* **2012**, *108*, 163002.

(41) Debye, P. *Polar Molecules*; Chemical Catalog Company: New York, 1929.

(42) Chizhik, A. I.; Chizhik, A. M.; Kern, A. M.; Schmidt, T.; Potrick, K.; Huisken, F.; Meixner, A. J. *Phys. Rev. Lett.* **2012**, *109*, 223902.